Volume holographic telescope

Arnab Sinha and George Barbastathis

Department of Mechanical Engineering and Microsystems Technology Laboratories, Massachusetts Institute of Technology, Room 3-461c, 77 Massachusetts Avenue, Cambridge, Massachusetts 02139

Received March 19, 2002

We have developed a novel imaging instrument, the volume holographic telescope, which is capable of returning high-resolution depth information about remote objects. We present a theoretical analysis of the instrument's performance and an experimental demonstration with a microfabricated object. © 2002 Optical Society of America

OCIS codes: 110.0110, 110.6770, 090.7330.

Volume holographic (VH) imaging utilizes the Bragg selectivity of volume diffraction to produce images of objects in four dimensions (three spatial and one spectral).[1,2] An information theoretic comparison[3] of a VH imaging system with a pinhole-based confocal system shows that volume holograms make better use of the optical power transmitted through the system's aperture [which is quantified by the numerical aperture (NA) of the system]. To date, volume holograms have been demonstrated as imaging elements in spectral imagers[2] and confocal microscopes.[4] In this Letter we present a method for obtaining $2^1/_2$-dimensional object information[5] from distant objects by use of a VH telescope. We concentrate on active imaging systems in which a reflective target is illuminated by laser light.

Figure 1 is a schematic of VH imaging for remote objects. The hologram is prerecorded, as shown in Fig. 1(a). The reference beam starts as a point source that is imaged by the telescope to a location in front of the hologram. The longitudinal distance of the reference point source from the entrance pupil of the telescope defines the range of the VH telescope, which can be varied to meet specific requirements. The signal beam is an off-axis plane wave. The volume hologram is the three-dimensional interference pattern of the two beams.

The imaging process is depicted in Fig. 1(b). The signal beam is blocked, and a single-element intensity detector is placed in the path of the beam diffracted by the volume hologram. A high value of measured intensity indicates the presence of a reflective surface at the input focal point of the VH imaging system. The object surface in its entirety is acquired by scanning of the object space voxel by voxel. The maximum depth of the system is determined by the available scanning range. We discuss the resolution below.

To understand the operation of the system we consider its two components (volume hologram and telescope) individually. The lateral[6] and longitudinal resolution of a stand-alone volume hologram (of thickness $L = 2$ mm, corresponding to that of the $LiNbO_3$ crystal used in the experiments) expressed in terms of the full width at half-maximum (FWHM) of the point-spread function (PSF) are given by

$$\Delta x_{\mathrm{FWHM}} \approx \frac{0.5\lambda}{\theta \times \mathrm{NA}}, \qquad \Delta z_{\mathrm{FWHM}} \approx \frac{1.7\lambda}{\mathrm{NA}^2}. \tag{1}$$

In expressions (1), θ is the angle that the off-axis signal beam makes with the optical axis, NA is the numerical aperture of the volume hologram, and λ is the operating wavelength. Figure 2 is a plot of theoretical values and experimental observations of Δz_{FWHM} for several values of the NA for the hologram.

For an imaging system with a fixed physical aperture, the NA decreases as the distance to the object increases. This means that resolution (lateral as well as longitudinal) degrades with increasing object distance but that the longitudinal degradation is worse because it scales quadratically according to expressions (1). One way to solve this problem is to increase the physical aperture of the system. This would be costly and impractical for a VH element. Instead, we insert a telescope in front of the hologram to produce a spatially demagnified secondary real image of the object in front of the hologram.

Another way to think about this solution is that the spatial demagnification of the image results in an enhancement of the bandwidth (BW) of the secondary image according to

$$\mathrm{BW}_{\mathrm{hol}} = \mathrm{BW}_{\mathrm{tel}} \times M_\alpha, \tag{2}$$

where M_α refers to the angular magnification of the telescope. The resolution of the system is not affected by the choice of magnification; it is still given by expressions (1), with NA being the entrance aperture of the telescope. Figure 3 shows experimentally obtained PSFs obtained for a point source for a fixed

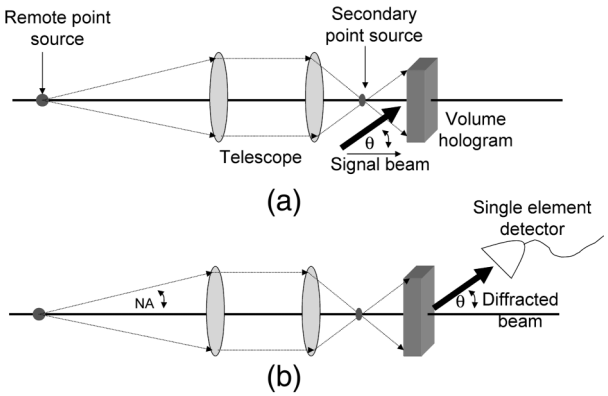

Fig. 1. Schematic of the VH telescope: (a) recording setup, (b) imaging setup.

0146-9592/02/191690-03$15.00/0

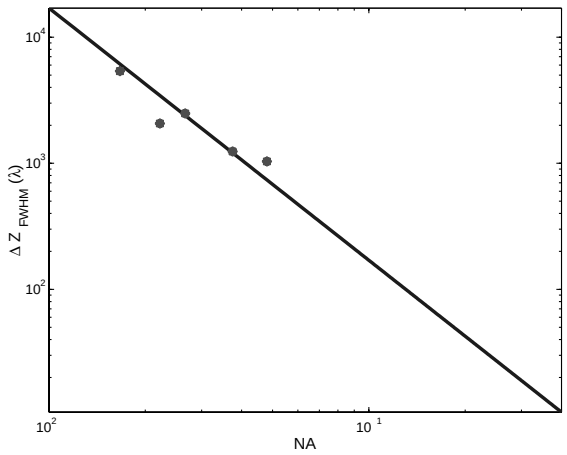

Fig. 2. Longitudinal resolution of the VH telescope: solid curve, theoretical; filled circles, experimental.

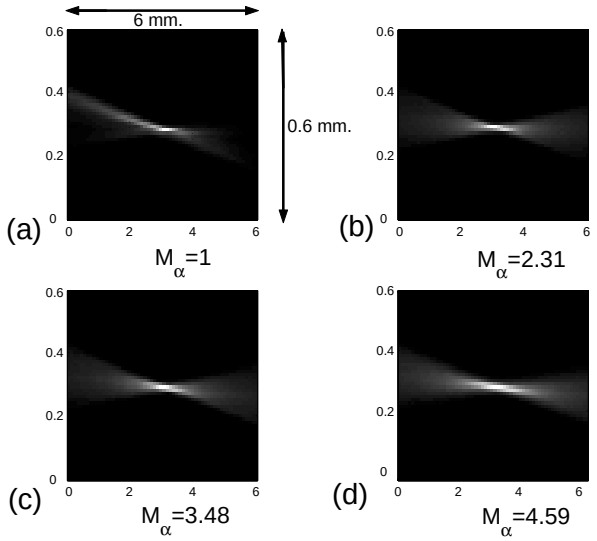

Fig. 3. VH telescopic PSFs obtained for VH telescopes with several magnifications for a point source object located 29 cm in front of the telescope. In these and subsequent experiments the holographic material was a 2-mm-thick slab of 0.03% Fe-doped $LiNbO_3$ recorded with a spherical wave reference and a plane-wave signal beam, $\theta = 30°$. The diffraction efficiency, η, was ~10%. The diameter of the front lens was 2.54 cm. The FWHMs of these PSFs were $\Delta z_{\mathrm{FWHM}} \sim 150\ \mu$m and $\Delta x_{\mathrm{FWHM}} \sim 15\ \mu$m.

distance and aperture size with four angular magnifications ($M_\alpha = 1, 2.31, 3.48, 4.59$). It can be observed that Δz_{FWHM} and Δx_{FWHM} are independent of M_α and depend solely on the NA of the system.

We used the VA telescope technique to obtain an image of a microturbine fabricated at the Microsystems Technology Laboratories, Massachusetts Institute of Technology. The reference beam was produced by reflection of a point source off an ordinary mirror. The theoretical value of the depth resolution at this distance was ~100 μm. The surface of the turbine had features that were ~225 μm deep. The turbine was placed 16 cm away from the entrance pupil of the telescope and was mounted upon a Newport linear three-axis translation stage. Scanning was carried out with a voxel size of 100 μm^3 over a volume of 5 mm^3 in the object space and three with Newport CMA-25CCCL actuators (one for each axis) controlled by a Newport ESP 300 motion controller. An ordinary camera would not provide depth resolution at this distance. The VH telescope was able to capture the microturbine surface layer by layer, as shown in Figs. 4(c)–4(f). Figure 4(c) is a scan of the base of the object. It can be seen that the base of the structure is Bragg matched and appears bright. However, the top surface appears dark as a result of Bragg mismatch. Figures 4(d) and 4(e) depict scans at progressive increments of 100 μm. As the base is raised, it gradually becomes Bragg mismatched and darker, whereas the opposite effect is observed for the top surface. This contrast reversal is complete in Fig. 4(f). The top surface is now completely Bragg matched and bright, and the base is completely Bragg mismatched and dark.

A single camera would not yield depth information for a similar setup. However, it is possible to obtain depth information by triangulating two camera pictures of the object at different angles with respect to the optical axis, as shown in Fig. 5. To compare the binocular imaging system with the VH telescope of

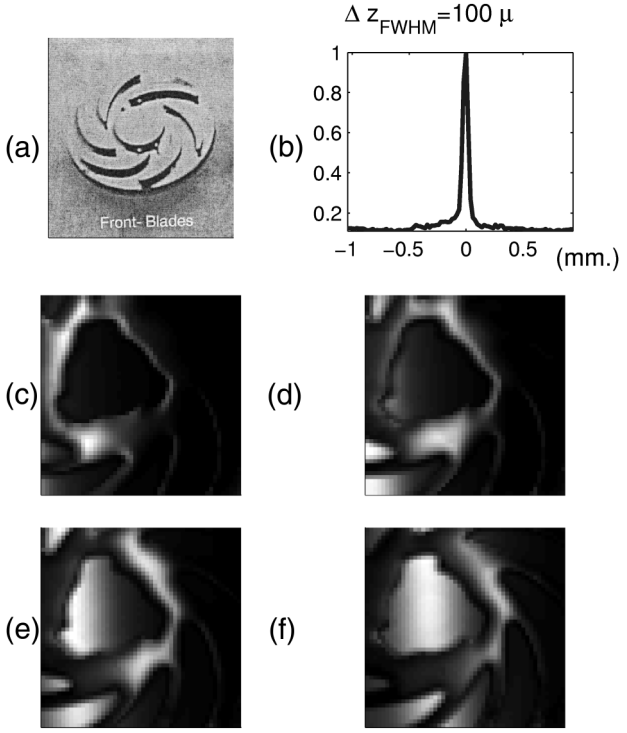

Fig. 4. Image of a silicon microturbine obtained with a VH telescope. The telescope had $M_\alpha = 1.5$, and the NA of the system was ~3.581°. The microturbine was located 16 cm away from the entrance pupil of the telescope. (a) Image of the microturbine captured with a standard digital camera. (b) Longitudinal PSF of the VH imaging systems for a Bragg-matched point source 16 cm away from the entrance pupil of the telescope: experimental, $\Delta z_{\mathrm{FWHM}} \sim 100\ \mu$m; theoreticcal, $\Delta z_{\mathrm{FWHM}} = 105\ \mu$m. (c)–(f) VH telescope scans at different depths through the object. At any given depth, the Bragg-matched portions of the object are brightest.

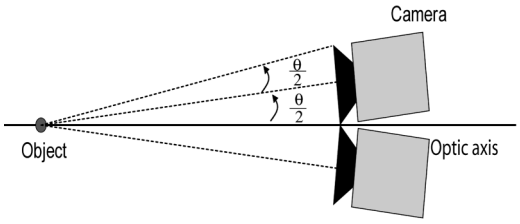

Fig. 5. Binocular imaging system for comparison with a VH telescope of equivalent NA.

Fig. 4 it is important to ensure that the two systems operate with the same NA. Thus we assume that the half-angle subtended by each camera is equal to the NA of the VH telescope, i.e., that $\sin(\theta/2) = \mathrm{NA}$. The depth resolution of the binocular system is given by

$$\Delta z_{\mathrm{FWHM}} = \frac{\Delta x_{\mathrm{FWHM}} \times M_{\alpha}}{\tan(\theta/2)}, \tag{3}$$

where Δx_{FWHM} is the diffraction-limited lateral resolution of the camera. For the geometry of Fig. 5 the lateral resolution is limited by the aperture of the camera and is given by

$$\Delta x_{\mathrm{FWHM}} = 0.61\lambda/\mathrm{NA}_c, \tag{4}$$

where $\mathrm{NA}_c = \sin(\theta/2)$ is the NA of each individual camera. Substituting Eq. (4) into Eq. (3) yields the value $\Delta z_{\mathrm{FWHM}} \sim 250\ \mu\mathrm{m}$. Thus we see that the VH telescope has better longitudinal resolution than a standard binocular arrangement of the same NA.

In conclusion, we have demonstrated depth-selective imaging at moderate distances by using a volume holographic lens in tandem with a telescope. The depth resolution is seen to obey the inverse square law that is seen in most systems and can resolve depth. However, the VH telescope makes better use of the available NA, as one can see by comparing the longitudinal resolution with that of an equivalent binocular triangulation system. Our preliminary studies indicate that VH telescopes may also be triangulated for further improvements in resolution. Efforts to demonstrate this effect are under way in our laboratory.

This research was supported by the U.S. Air Force Research Laboratories (Eglin Air Force Base, Munitions & Ordnance Division, AFRL/MNG). We are grateful to Chee-Wei Wong for providing the microturbine and to Andy Stein for helpful discussions. The authors' e-mail addresses, in order, are arnab@mit.edu and gbarb@mit.edu.

References

1. G. Barbastathis and D. J. Brady, Proc. IEEE **87,** 2098 (1999).
2. W. Liu, G. Barbastathis, and D. Psaltis, Opt. Lett. **27,** 854 (2002).
3. G. Barbastathis and A. Sinha, Trends Biotechnol. **19,** 383 (2001).
4. G. Barbastathis, M. Balberg, and D. J. Brady, Opt. Lett. **24,** 811 (1999).
5. D. Marr, *Vision: A Computational Investigation into Human Representation and Processing of Visual Information* (Freeman, San Francisco, Calif., 1982).
6. G. Barbastathis and D. Psaltis, in *Holographic Data Storage*, H. J. Coufal, D. Psaltis, and G. T. Sincerbox, eds., Vol. 76 of Springer Series in Optical Sciences (Springer-Verlag, Berlin, 2001), pp. 21–62.